IOP Publishing Physica Scripta
Phys. Scr. 95 (2020) 035505 (8pp) https://doi.org/10.1088/1402-4896/ab4b9f

Infrared subwavelength focusing metasurfaces for harvesting heat from the Earth's back radiation

Manar Abdel-Galil[1,2,4], Yehea Ismail[1] and Mohamed Swillam[3]

[1] Center for Nanoelectronics and Devices, American University in Cairo/Zewail City of Science and Technology, Cairo, Egypt
[2] Department of Electrical and Communications Engineering, Faculty of Engineering, Ain Shams University, Cairo, Egypt
[3] Department of Physics, School of Science and Engineering, American University in Cairo, New Cairo, 11835, Egypt

E-mail: manar.mansour@aucegypt.edu

Received 16 May 2019, revised 22 September 2019
Accepted for publication 7 October 2019
Published 3 February 2020

Abstract

In this paper, we introduce two different metasurfaces that can achieve subwavelength focusing of the electromagnetic radiation in the infrared range with transmission efficiencies reaching 46% and 74.33% in silicon and thus they can be integrated in heat harvesting applications. We made our designs at the wavelength of 10 μm which is the peak of the back radiation of the Earth. In designing our metasurfaces in the infrared range, we used the phase modulation techniques that proved to be useful in the visible domain. The best focusing resolution achieved in our metasurfaces is 0.26λ (super-focusing). In addition to heat harvesting, the two proposed metasurfaces can be useful in other compact applications that require manipulating the mid-infrared radiation on a very small scale. We used copper and silicon in our metasurfaces which are specifically suitable for the mid-infrared range besides being CMOS compatible. In this paper, we also explained how heat can be harvested from the introduced metasurfaces using the Seebeck effect.

Keywords: mid-infrared focusing, metasurface, planar lens, subwavelength focusing, plasmonics, phase modulation, heat harvesting

(Some figures may appear in colour only in the online journal)

1. Introduction

The mid-infrared spectral range of 2–20 μm contains the absorption fingerprints of the most common molecular vibrations which makes it possible to study the chemical composition of different materials in this range. However, it remained a neglected part of the spectrum, even for spectroscopy, until the introduction of devices like quantum cascade lasers and quantum-well infrared photodetectors [1–4].

The mid-infrared silicon photonics is a new research domain that is still less developed than the near-infrared or the visible domains. More research efforts still need to be done in order to fully exploit the potential of this range. Although the mid-infrared range covers a large wavelength domain, there is still no material platform to be used in the whole range [5].

According to the diffraction theory, when light passes through a subwavelength aperture, it diffracts in all directions and has weak transmission [6]. This puts a limitation on the smallest feature size that could be achieved in integrated photonic circuits or systems. However, in 1998, Thomas Ebbesen found that an opaque screen perforated with a number of subwavelength holes transmitted more light than what was expected from the total area of the holes. This phenomenon was referred to as extraordinary optical transmission [7]. Subsequent studies showed that the phenomenon could be attributed to the excitation of surface plasmon polaritons [8, 9]. Following the discovery of this

[4] Author to whom any correspondence should be addressed.

phenomenon, many subwavelength optical devices and metasurfaces were made such as the plasmonic lens which was extensively studied in the recent years [10–25]. Different phase modulation approaches were used to make subwavelength focusing lenses in the visible range. Those techniques include depth modulation [11], width modulation [13, 15], refractive index modulation of the filling material [16], both width and refractive index modulation [14] and finally initial phase modulation [17].

Most of the research efforts were first directed towards studying the plasmonic effect in the visible range and building structures that can manipulate light in this range; however, the interest is now extending to the mid-infrared range as well [1]. It was challenging to transfer the knowledge acquired in visible plasmonics to the mid-infrared domain because the materials have different response in the mid-infrared than in the visible range [26].

In our work, we built two metasurfaces that act as focusing lenses in the mid-infrared range. They are based on two different phase modulation techniques that were employed in the visible range [13–15]. The proposed metasurfaces can achieve subwavelength focusing of mid-infrared radiation in silicon with transmission efficiencies reaching 46% and 74.33%.

The ability to focus the mid-infrared radiation with high transmission efficiency would be useful for different heat harvesting applications. It can also be useful in medical diagnosis and non-invasive health checks. In addition, most molecules have unique absorption lines or signature in the mid-infrared range which could facilitate the study and analysis of many gases and biological molecules. Sensing, thermal photovoltaic cells, infrared integrated cameras, environmental monitoring and control are also possible applications of the mid-infrared range [1, 27].

Focusing at $\lambda = 4.6$ μm in the mid-IR with high transmission efficiency was reported in [28] but the measured focused beam size is close to 156 μm which is far greater than the wavelength. Also the structure is made of gold which is relatively expensive.

Our proposed metasurfaces are specifically advantageous and well suited for silicon based heat harvesting applications as explained in section 2.

Heat harvesting can be achieved in our designs using the Seebeck effect where we create a thermal gradient by focusing the mid-infrared radiation into a hot spot which would be surrounded by a cold region.

The paper is organized as follows: A theoretical background is explained in section 2, the two metasurfaces are given in section 3, simulation results are shown in section 4, the proposed fabrication steps of the metasurfaces are displayed in section 5, harvesting heat from the focused radiation using seebeck effect is explained in section 6 and finally the paper is concluded in section 7.

2. Theoretical background

The propagation constant β of the plasmonic mode in a subwavelength metallic slit of width w and depth d is given by the relation [13]

$$\tanh\left(\sqrt{\beta^2 - {k_o}^2\varepsilon_d}\,\frac{w}{2}\right) = \frac{-\varepsilon_d\sqrt{\beta^2 - {k_o}^2\varepsilon_m}}{-\varepsilon_m\sqrt{\beta^2 - {k_o}^2\varepsilon_d}}, \qquad (1)$$

where k_o is the wave vector of the incident wave in free space, ε_m and ε_d are the relative dielectric constants of the metal and the dielectric material filling the slit respectively, and w is the width of the slit.

If we have a number of slits in tandem, we can get a focusing effect by designing the slits such that they give different phase retardations to the incident wave in order to get a curved wavefront in the output.

Phase modulation can be done by varying either the slit depth d as in [11] or the propagation constant β. The lens based on depth modulation faces the same fabrication difficulties of the conventional glass lenses which are non-planar surfaces [16].

From equation (1), the propagation constant β can be modulated by varying the slit width w as in [13, 15] or the refractive index of the dielectric material filling the slit i.e. ε_d as in [16] or by varying both w and ε_d as in [14] assuming we are using a certain metal with a dielectric constant ε_m.

When we have a number of subwavelength slits placed in tandem, in order for the output waves to reach the focal point in phase, the phase delay should satisfy the following equation of the equal optical length principle

$$\mathrm{f}(x) = 2n\pi + \frac{2\pi f}{\lambda} - \frac{2\pi\sqrt{f^2 + x^2}}{\lambda}, \qquad (2)$$

where n is an arbitrary integer, λ is the wavelength of the incident radiation and f is the focal length.

In our proposed metasurfaces in the infrared, we adopted two of the phase modulation approaches which were used in the visible range: the approach of both slit width modulation and refractive index modulation of the filling material in the slits [14], and the approach of slit width modulation only [13, 15].

In case of slit width modulation only, we have a number of slits increasing in width from the central slit to the side slits so each slit experiences a different phase shift such that we get a curved wavefront in the output. The wave is slower inside the narrower slits at the middle of the structure since most of the plasmonic mode resides in the metal. Therefore, the middle slits introduce higher phase delay than the side slits which are wider in width.

In case of the other approach of varying both the slit width and refractive index of the filling material in the slits, we have an extended phase delay range which leads to improving the focusing performance where the light intensity is greatly enhanced at the focus [14].

Width-modulated planar lenses in the visible range face a fabrication difficulty because the slits which are narrower than 30 nm are very difficult to fabricate in a thick metal film [14]. However, this problem is not encountered in our mid-infrared designs because the dimensions in the mid-infrared range are greater and thus will not face the same fabrication difficulty

Figure 1. The first metasurface (MS1) based on the approach of both slit width modulation and refractive index modulation of the filling materials in the slits.

Table 1. The extinction coefficients of copper, SILVER AND GOLD at the wavelength of 10 μm.

Metal	Extinction coefficient
Copper (Cu)	49
Gold (Au)	53.4
Silver (Ag)	71.9

faced by the width-modulated planar lenses in the visible range.

We used copper as a metal to build our metasurfaces for two reasons. First, it has lower absorption losses in the mid-infrared range compared to the traditional metals used in visible plasmonics such as silver or gold. Table 1 shows the extinction coefficient of copper, gold and silver at the mid-infrared wavelength of 10 μm based on the model in [29]. Copper has the least extinction coefficient which accounts for the absorption losses. Copper is also cheaper compared to gold or silver or other metamaterials used in focusing.

The second reason why we chose copper is its CMOS compatibility so the proposed metasurfaces can be integrated in CMOS applications.

3. The metasurface designs

3.1. First approach: both width and material modulation

The first metasurface (MS1) shown in figure 1 is based on the technique of both width and refractive index modulation [14]. The body of the lens is a copper film of depth $d = 1$ μm. The diameter of the lens aperture is $D = 30$ μm. There are 13 slits (6 slits on each side of the central slit). The metasurface is symmetrical about the central slit. The slits range in width from 0.8 μm at the center of the structure to 1.5 μm on the side and are spaced 2 μm apart. The detailed values of the slit positions, widths and filling materials are shown in table A1 in appendix. The table gives only the details of the upper half of the metasurface since the structure is symmetrical. All the slits are filled with air except the three slits at the center and each two slits on the side which are filled with silicon as shown in figure 1. The wavelength of the plane wave incident from the left side of the lens is $\lambda = 10$ μm (the peak wavelength of the back radiation of the Earth). At this wavelength, the relative permittivity of copper is $\varepsilon_m = -2342.48 + i\ 1059.9$ [29] and the refractive index of silicon is 3.42. A summary of the metasurface parameters is shown in table 2.

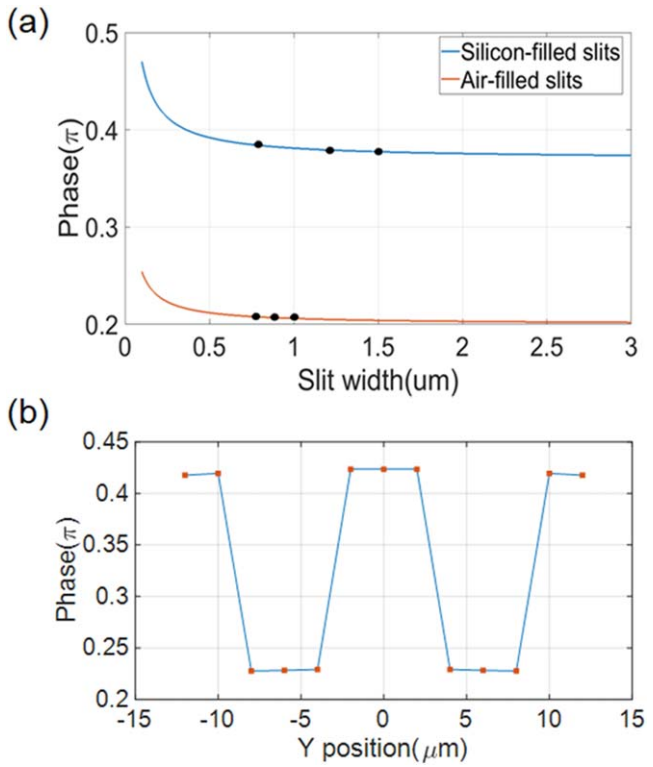

Figure 2. The variation of the phase delay with the slit width for MS1 in case of silicon filling and air filling. (b) The phase variation across the vertical position of the slits where the slits occur at the positions marked in red on the phase curve.

Table 2. Design parameters of MS1.

Parameter	Value
Working wavelength (λ)	10 μm
Slit depth (d)	1 μm
Diameter of the lens aperture (D)	30 μm
Total number of slits (N)	13

Plotting the phase versus the slit width once at $\varepsilon_d = 1$ (air filling) and then at $\varepsilon_d = 3.42$ (silicon filling), we get the two curves shown in figure 2(a). The chosen slit widths are marked on both curves. Figure 2(b) also shows the phase variation across the vertical position of the slits where the slits occur at the positions marked on the curve.

3.2. Second approach: width modulation only

The second metasurface (MS2) shown in figure 3 is based on the technique of slit width modulation only [13, 15].

The body of the lens is a copper film of depth = 2.5 μm. The detailed values of the slit positions and widths are shown in table A2 in appendix. The material filling the slits is only air. The wavelength of the plane wave incident from the left

Figure 3. The second metasurface (MS2) based on width modulation only.

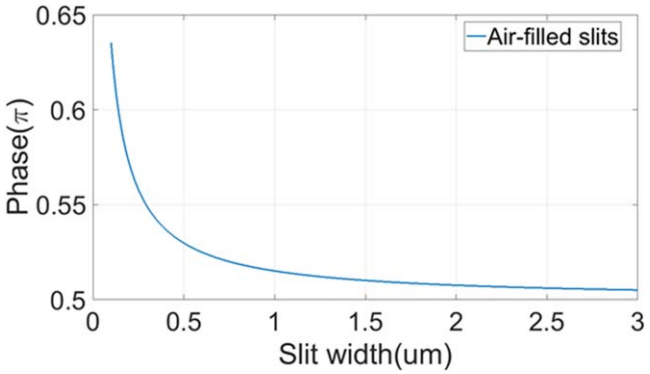

Figure 4. The variation of the phase delay with the slit width for MS2 whose slits are only filled with air.

Table 3. Design parameters of MS2.

Parameter	Value
Working wavelength (λ)	10 μm
Slit depth (d)	2.5 μm
Diameter of the lens aperture (D)	30 μm
Total number of slits (N)	13

side of the lens is $\lambda = 10$ μm. A summary of the metasurface parameters is shown in table 3. Plotting the phase versus the slit width, we get curve shown in figure 4.

4. Simulation results

A commercial-grade simulator based on the finite-difference time-domain method was used to perform the calculations [30] and the following results were obtained.

Figure 5 shows the magnetic field intensity profile and a vertical cross-section passing through the focus center for MS1. Similarly, figure 6 shows the results for MS2.

In case of MS1, the focal length was found to be 19.5 μm and the FWHM is 2.64 μm which is almost quarter the wavelength of the incident mid-incident infrared wave

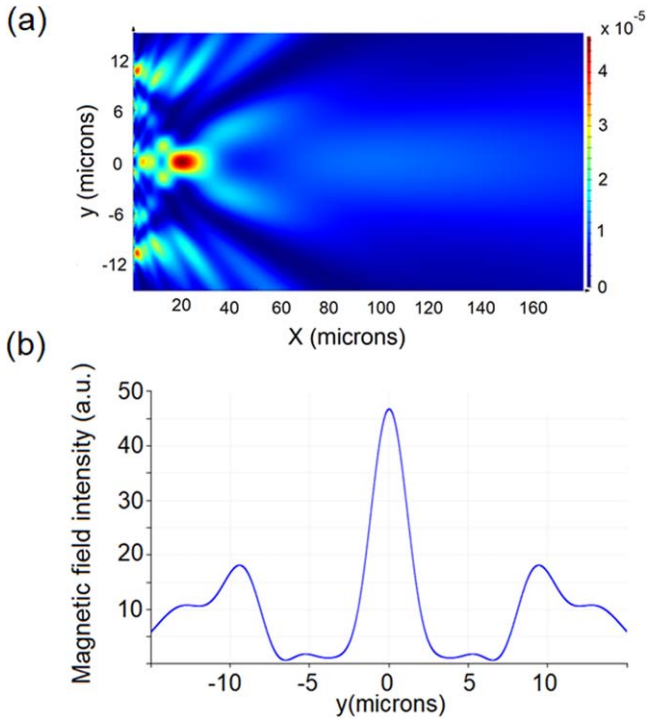

Figure 5. (a) The magnetic field intensity distribution $|H|^2$ of the focused radiation in case of MS1. The field intensity is measured in arbitrary units. (b) A vertical cross-section passing through the center of the focus for the magnetic field intensity of MS1. The field intensity is measured in arbitrary units.

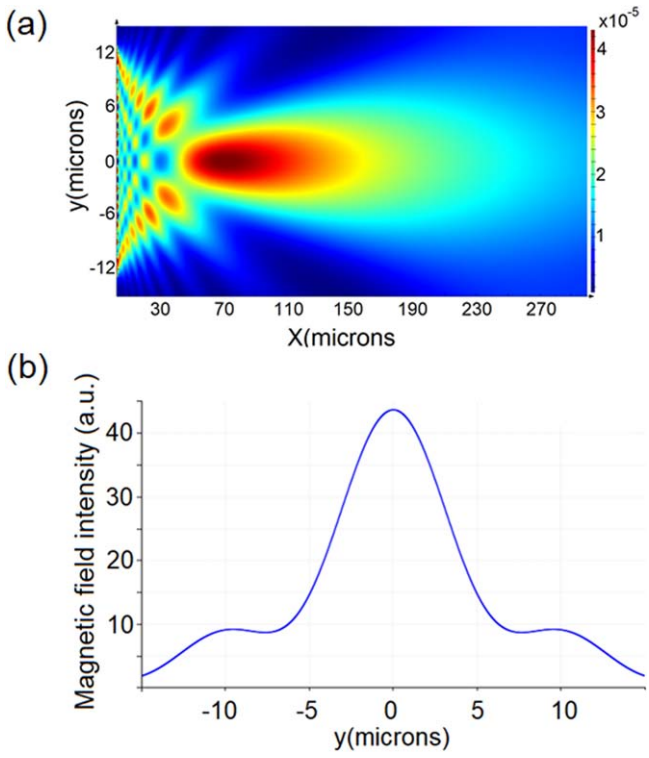

Figure 6. (a) The magnetic field intensity distribution $|H|^2$ of MS2. The field intensity is measured in arbitrary units. (b) A vertical cross-section passing through the center of the focus for the magnetic field intensity of MS2. The field intensity is measured in arbitrary units.

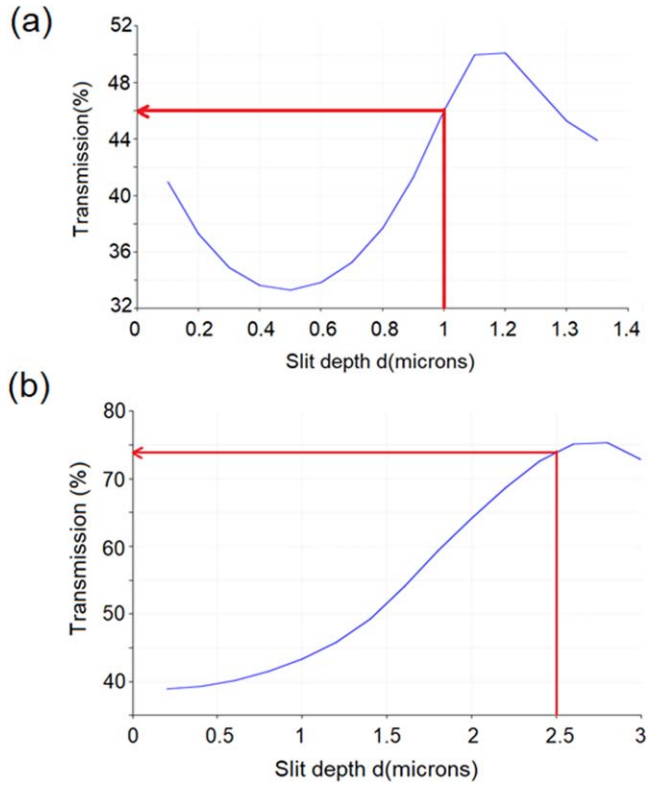

Figure 7. (a) The transmission percentage versus the slit depth in microns for MS1. (b) The transmission percentage versus the slit depth in microns for MS2.

($\lambda = 10$ μm) and thus we have super focusing. The attained transmission efficiency is 46% (the input is TM-mode).

In case of MS2, the focal length was found to be 68.5 μm and the FWHM is 7.76 μm which is still smaller than the wavelength of the incident mid-infrared wave. The attained transmission efficiency is 74.33% (the input is TM-mode).

For both metasurfaces, the transmission varies with the slit depth. We showed this fact by plotting the transmission percentage versus the slit depth for both metasurfaces as shown in figure 7.

It should be noted that the focusing performance is not the same for all the transmission values. We noticed that it usually degrades at very high or low transmission so it is up to the designer to choose whether they prefer to have very high transmission at the expense of the focusing performance or the other way around.

We designed our metasurfaces at the two points traced in red on the two curves in figure 7 because they are the optimum points with regard to both the focusing performance and the transmission efficiency.

5. Proposed fabrication steps of the metasurfaces

The two proposed metasurfaces in section 3 can be easily fabricated using two microfabrication processes which are etching and lift-off. MS1 would require both etching and lift-off while MS2 would only require a lift-off process. The fabrication steps of MS2 are shown in figure 8 while the fabrication steps of MS1 are shown in figure 9. In step (g) of figure 9, the photoresist has to be high enough to prevent the overlapping of the copper in the gaps and the copper on the top surface of the photoresist. This overlapping would prevent the completion of the lift-off process.

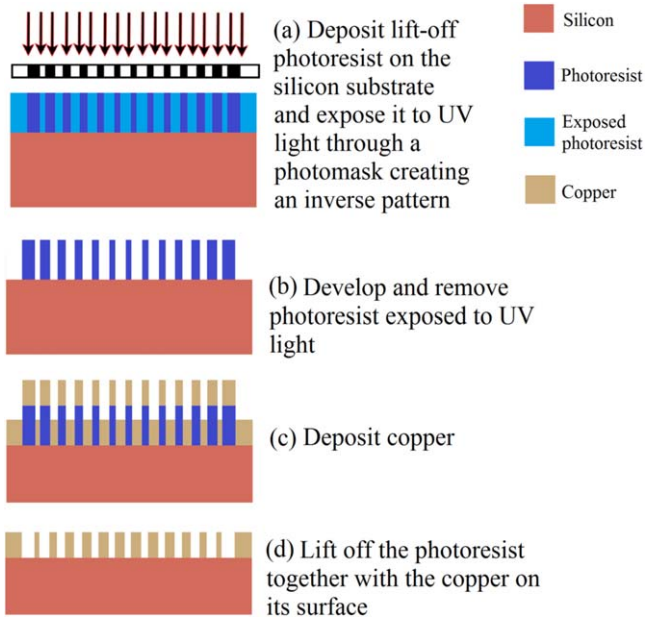

Figure 8. The lift-off process used to fabricate MS2.

6. Harvesting heat from the focused radiation using seebeck effect

Thermoelectric generators are solid-state devices that can convert heat energy into electricity when we have a thermal gradient between two dissimilar conductors [31]. This effect is called the Seebeck effect after Thomas Johann Seebeck who discovered it in 1821 [32]. As illustrated in figure 10, the thermoelectric module is composed of two dissimilar thermoelectric materials which are a p-type (having free holes) and an n-type (having free electrons) semiconductors connected at their ends. The heat flow resulting from the thermal gradient in the thermoelectric material leads to the diffusion of the mobile charge carriers between the hot and cold surfaces creating a voltage difference. Therefore, the thermoelectric generator can be used to deliver electric power to an external load connected to it. The current flow that occurs is due to the fact that the free carriers in the semiconductor carry charge as well as heat while they diffuse from the hot to the cold end [33].

The voltage difference obtained across the load is given by

$$\Delta V = -S\Delta T, \tag{3}$$

where S is the Seebeck coefficient and ΔT is the temperature difference across the thermoelectric material. The current

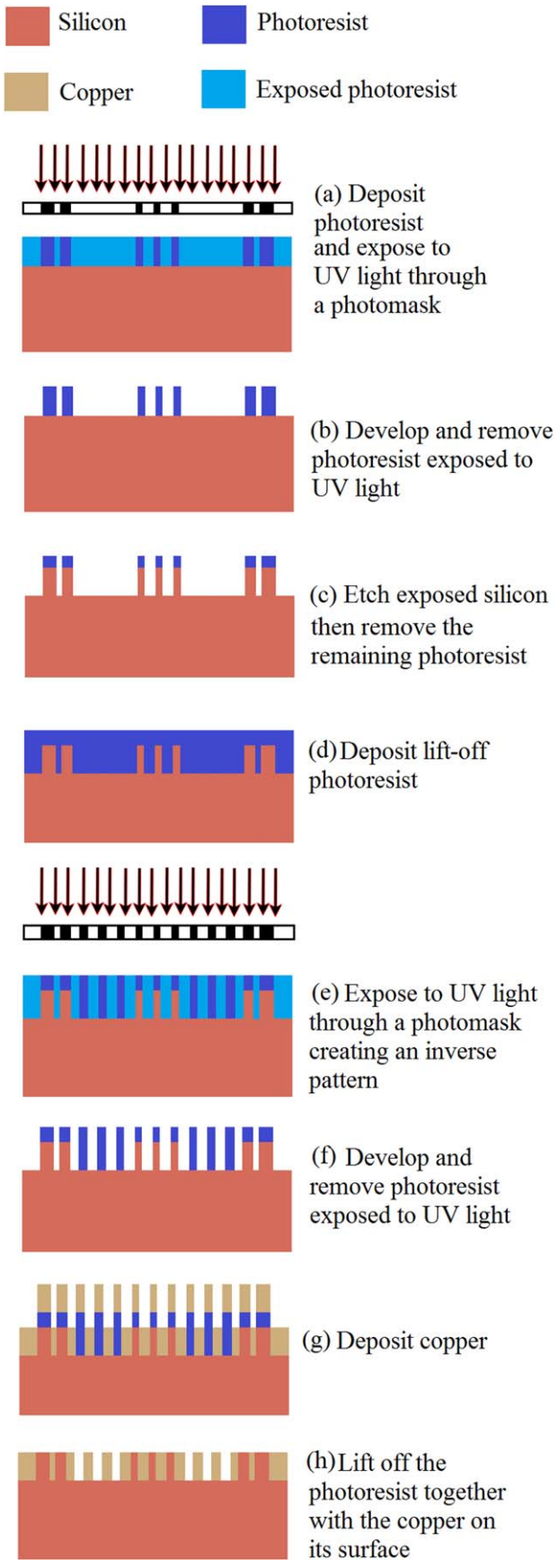

Figure 9. The etching and lift-off processes used to fabricate MS1.

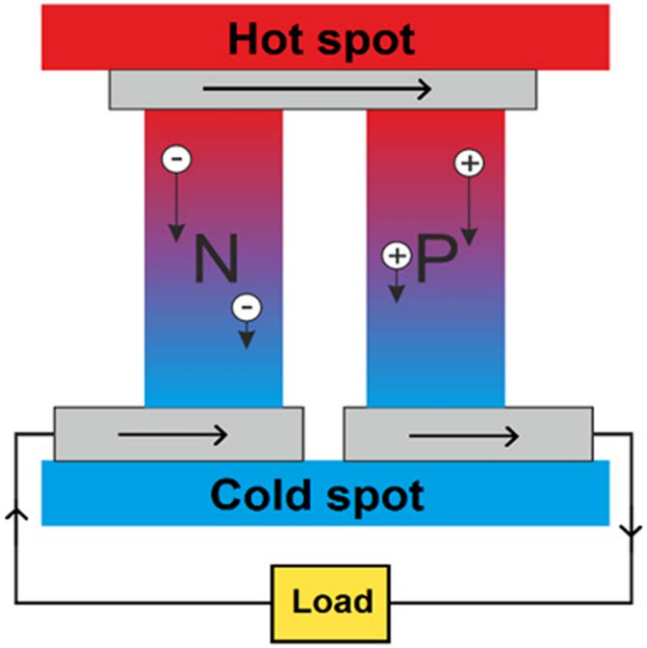

Figure 10. An illustration of heat harvesting using Seebeck effect.

generated as a result of the temperature difference across the thermoelectric generator is given by [34]

$$I = \frac{S\Delta T}{R_{TE} + R_e}, \tag{4}$$

where R_{TE} and R_e are the electrical resistance of the thermoelectric generator and the external load resistance respectively.

The power delivered to the external load is given by

$$P = I^2 R_e = \frac{S^2 \Delta T^2 R_e}{(R_{TE} + R_e)^2}. \tag{5}$$

Differentiating the power with respect to the load resistance leads to the condition of maximum power transfer known as impedance matching [34]

$$R_e = R_{TE}. \tag{6}$$

This implies that maximum power is delivered to the external load resistance and in this case the maximum thermoelectric generator when its internal resistance is equal to the power is given by [34]

$$P_{\max} = \frac{S^2 \Delta T^2}{4R_{TE}}. \tag{7}$$

Therefore, we conclude that in order to obtain maximum power at the load, the internal resistance of the thermoelectric generator should match the load resistance. We also notice that the maximum power itself is directly proportional to the square of both the Seebeck coefficient and the temperature difference and is inversely proportional to the internal resistance of the thermoelectric generator which means we

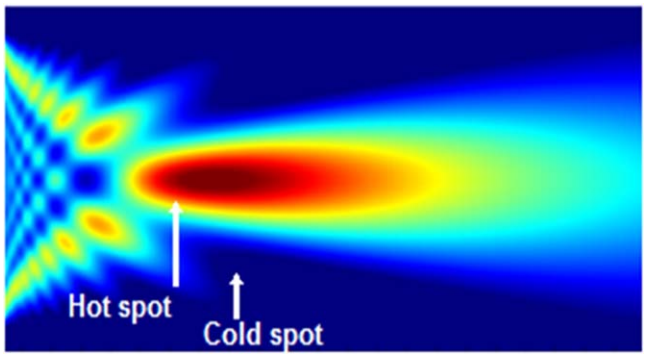

Figure 11. An illustration of the hot and cold regions in our lens structures which are necessary for thermoelectric generation using Seebeck effect.

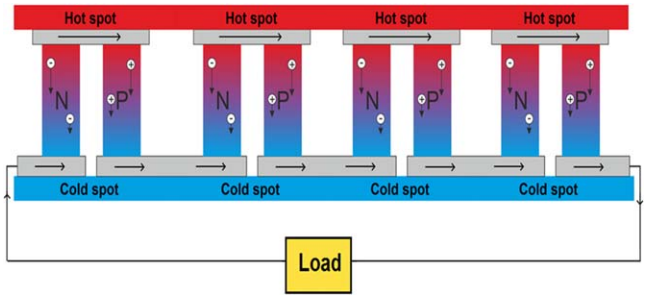

Figure 12. An illustration of a thermoelectric generator consisting of three thermoelectric couples connected electrically in series and thermally in parallel.

can increase the maximum power driven from the thermoelectric generator by minimizing its internal resistance, maximizing the temperature gradient and choosing a thermoelectric material with the highest possible Seebeck coefficient.

In our metasurfaces proposed in section 3, the region where the mid-infrared radiation is focused will act as the hot surface while any other region where there is no focusing will act as the cold surface as illustrated in figure 11. Many metasurfaces can be placed in tandem to make several thermoelectric couples which should be connected electrically in series and thermally in parallel to obtain a considerable voltage difference at the load [31]. Figure 12 shows an example of a thermoelectric generator consisting of three thermoelectric couples connected electrically in series and thermally in parallel.

7. Conclusion

In this paper, two different metasurfaces were introduced that can achieve subwavelength focusing of the mid-infrared radiation with transmission efficiencies reaching reaching 46% and 74.33% in silicon at the wavelength of 10 μm (the peak wavelength of the back radiation of the Earth). The metasurfaces are based on two different phase modulation techniques. The first metasurface which is based on both slit width and refractive index modulation achieves a FWHM $= 2.64$ μm and a transmission efficiency of 46% in silicon while the second metasurface which is based only on slit width modulation achieves a FWHM $= 7.76$ μm and a transmission efficiency of 74.33% in silicon. We noticed that there is a general trade-off between the focusing resolution and the transmission efficiency. For certain applications like heat harvesting, it would be desirable to have high transmission efficiency while for other applications like lithography the focusing resolution would be critical. Therefore, the metasurfaces introduced in this paper can serve in different applications according to the critical requirement of the application itself. The proposed metasurfaces are well suited for integration in heat harvesting, sensing, medical diagnosis and different silicon based applications. We also showed how the transmission efficiency varies with the slit depth in both metasurfaces. Finally, we explained how the proposed metasurfaces can be easily fabricated using etching and lift-off processes and we showed in principle how those metasurfaces can be used in heat harvesting based on Seebeck effect.

Acknowledgments

This work has been partially supported by the fund received from Egyptian academy of scientific research and technology (ASRT), under the grant titled ‘Innovation Management cluster for local manufacturing of industrial electronic components (DLMEI)’

Appendix

Detailed tables

Table A1. The slit positions, widths and filling materials in MS1.

Slit number	Slit position in microns (along the vertical axis)	Slit width in microns	Filling material in the slit
0	0	0.8	Silicon
1	2	0.8	Silicon
2	4	0.8	Air
3	6	0.9	Air
4	8	1	Air
5	10	1.2	Silicon
6	12	1.5	Silicon

Table A2. The slit positions, widths and filling materials in MS2.

Slit number	Slit position in microns (along the vertical axis)	Slit width in microns	Filling material in the slit
0	0	0.8	Air
1	2	0.8	Air
2	4	0.8	Air
3	6	0.9	Air
4	8	1	Air
5	10	1.2	Air
6	12	1.5	Air

ORCID iDs

Mohamed Swillam https://orcid.org/0000-0002-7962-2341

References

[1] Stanley R 2012 Plasmonics in the mid-infrared *Nat. Photon.* **6** 409–11

[2] Byrnes S J, Blanchard R and Capasso F 2014 Harvesting renewable energy from Earth's mid-infrared emissions *Proc. Natl Acad. Sci.* **111** 3927–32

[3] Faist J, Capasso F, Sivco D L, Sirtori C, Hutchinson A L and Cho A Y 1994 Quantum cascade laser *Science* **264** 553–6

[4] Levine B F 1993 Quantum-well infrared photodetectors *J. Appl. Phys.* **74** R1–81

[5] Thomson D *et al* 2016 Roadmap on silicon photonics *J. Opt.* **18** 073003

[6] Bethe H A 1944 Theory of diffraction by small holes *Phys. Rev.* **66** 163

[7] Ebbesen T W, Lezec H J, Ghaemi H F, Thio T and Wolff P A 1998 Extraordinary optical transmission through sub-wavelength hole arrays *Nature* **391** 667–9

[8] Yu L B, Lin D Z, Chen Y C, Chang Y C, Huang K T, Liaw J W, Yeh J T, Liu J M, Yeh C S and Lee C K 2005 Physical origin of directional beaming emitted from a subwavelength slit *Phys. Rev.* B **71** 041405

[9] Thio T, Pellerin K M, Linke R A, Lezec H J and Ebbesen T W 2001 Enhanced light transmission through a single subwavelength aperture *Opt. Lett.* **26** 1972–4

[10] Fu Y and Zhou X 2010 Plasmonic lenses: a review *Plasmonics* **5** 287–310

[11] Sun Z and Kim H K 2004 Refractive transmission of light and beam shaping with metallic nano-optic lenses *Appl. Phys. Lett.* **85** 642–4

[12] Garcıa-Vidal F J, Martın-Moreno L, Lezec H J and Ebbesen T W 2003 Focusing light with a single subwavelength aperture flanked by surface corrugations *Appl. Phys. Lett.* **83** 4500–2

[13] Shi H, Wang C, Du C, Luo X, Dong X and Gao H 2005 Beam manipulating by metallic nano-slits with variant widths *Opt. Express* **13** 6815–20

[14] Chen Q 2011 A novel plasmonic zone plate lens based on nano-slits with refractive index modulation *Plasmonics* **6** 381–5

[15] Verslegers L, Catrysse P B, Yu Z, White J S, Barnard E S, Brongersma M L and Fan S 2008 Planar lenses based on nanoscale slit arrays in a metallic film *Nano Lett.* **9** 235–8

[16] Gao Y, Liu J, Zhang X, Wang Y, Song Y and Liu S 2012 Metallic planar lens with binary nanoscale slits *IEEE Photonics Technol. Lett.* **24** 969–71

[17] Jia S, Wu Y, Wang X and Wang N 2014 A subwavelength focusing structure composite of nanoscale metallic slits array with patterned dielectric substrate *IEEE Photonics J.* **6** 1–8

[18] El Maklizi M, Hendawy M and Swillam M A 2014 Super-focusing of visible and UV light using a meta surface *J. Opt.* **16** 105007

[19] Abdel-galil M, Ismail Y and Swillam M A 2017 Subwavelength focusing in the infrared range using a meta surface *ACES Conf.* pp 1–2

[20] Schuller J A, Barnard E S, Cai W, Jun Y C, White J S and Brongersma M L 2010 Plasmonics for extreme light concentration and manipulation *Nat. Mater.* **9** 193–204

[21] Dragoman M and Dragoman D 2008 Plasmonics: applications to nanoscale terahertz and optical devices *Prog. Quantum Electron.* **32** 1–41

[22] Kawata S, Inouye Y and Verma P 2009 Plasmonics for near-field nano-imaging and superlensing *Nat. Photonics* **3** 388–94

[23] Wang Q, Zhang X, Xu Y, Tian Z, Gu J, Yue W, Zhang S, Han J and Zhang W 2015 A broadband metasurface-based terahertz flat-lens array *Adv. Opt. Mater.* **3** 779

[24] Khorasaninejad M, Aieta F, Kanhaiya P, Kats M A, Genevet P, Rousso D and Capasso F 2015 Achromatic metasurface lens at telecommunication wavelengths *Nano Lett.* **15** 5358–62

[25] Zhao Y, Lin S S, Nawaz A A, Kiraly B, Hao Q, Liu Y and Huang T J 2010 Beam bending via plasmonic lenses *Opt. Express* **18** 23458–65

[26] Law S, Podolskiy V and Wasserman D 2013 Towards nano-scale photonics with micro-scale photons: the opportunities and challenges of mid-infrared plasmonics *Nanophotonics* **2** 103–30

[27] Soref R 2010 Mid-infrared photonics in silicon and germanium *Nat. Photon.* **4** 495–7

[28] Zhang S *et al* 2016 High efficiency near diffraction-limited mid-infrared flat lenses based on metasurface reflectarrays *Opt. Express* **24** 18024–34

[29] Ordal M A, Long L L, Bell R J, Bell S E, Bell R R, Alexander R W and Ward C A 1983 Optical properties of the metals Al, Co, Cu, Au, Fe, Pb, Ni, Pd, Pt, Ag, Ti, and W in the infrared and far infrared *Appl. Opt.* **22** 1099–119

[30] Lumerical Inc (https://www.lumerical.com/)

[31] Snyder G J 2008 Small thermoelectric generators *Electrochem. Soc. Interface* **17** 54–6

[32] Seebeck T J 1825 Magnetische Polarisation der Metalle und Erze durch Temperatur-Differenz (Magnetic polarization of metals and minerals by temperature differences) *Abhandlungen der Königlichen Akademie der Wissenschaften zu Berlin* (Berlin: Treatises of the Royal Academy of Sciences) pp 265–373

[33] Snyder G J and Toberer E S 2008 Complex thermoelectric materials *Nat. Mater.* **7** 105–14

[34] Chen W, Wu P, Wang X and Lin Y 2016 Power output and efficiency of a thermoelectric generator under temperature control *Energy Convers. Manage.* **127** 404–15